Development of control laws for the simulation of a new transport aircraft

F Holzapfel[1]*, **M Heller**[1], **M Weingartner**[1], **G Sachs**[1], and **O da Costa**[2]
[1]Institute of Flight System Dynamics, TU München, Germany
[2]IABG mbH, Ottobrunn, Germany

The manuscript was received on 7 November 2007 and was accepted after revision for publication on 26 November 2008.

DOI: 10.1243/09544100JAERO309

Abstract: This article presents the development of fly-by-wire control laws used for the high-fidelity simulation of a new transport category aircraft. Beyond structural and gain design aspects for normal operations, envelope protections and limitations as well as mode transition issues are also addressed. As the control system is to be adjusted to changing aircraft datasets at different levels of fidelity, particular emphasis has been put on a high level of automation in gain design and system assessment routines. For lateral dynamics, eigenstructure assignment is used as the design methodology whereas pole placement is used for the pitch axis.

Keywords: flight control, transport aircraft, fly-by-wire

1 INTRODUCTION

With the availability of significant computing power, numerical simulation has become an important method to verify the capabilities of a new aircraft design during the stages of its development.

Such efforts are of interest not only to aircraft manufacturers but also to customers as they can continuously accompany and trace the development of the system and monitor the compliance with the original specifications and requirements based on own and independent simulations.

A restricting factor is the limited amount of data available from the manufacturer that introduces a degree of uncertainty into the process.

However, statements concerning tendencies and parameter changes are quite robust and help to properly predict the consequences of configuration changes like new mass and gross weight data, tank volumes, aerodynamic efficiencies, control surface sizing, lever arms, and so on. This gives the customer a solid and stable basis for planning his responses and reactions to manufacturer statements.

For modern fly-by-wire aircraft, the dynamic behaviour of the system, its operational envelope, its performance, and handling characteristics are determined by the flight control system (FCS) – of course within the physical limits provided by capabilities of the configuration and its subsystems.

As a consequence, the proper simulation of the FCS turns out to be an important aspect that has to be considered right from the beginning. Especially in flight phases like steep approaches, where the available envelope is fully exploited, or in precision tracking tasks, where bandwidth matters, the limitations and characteristics introduced by the FCS may not be neglected for representative analysis results.

As no manufacturer information is available on the internal structure of the FCS but only on the characteristics as seen from the pilot's point of view, a proprietarily developed structural design is to be performed. Thus, the FCS layout concerning feedbacks, command paths, and filters as well as the implementation of mode transitions has been developed independently from scratch.

The design is not performed for a flying aircraft but for one under development, where content, amount, and fidelity of the data available are subject to changes. To account for this, a high level of automation in system analysis, filter, and gain design as well as closed-loop assessment is of high importance to reduce the workload for recurring tasks.

The FCS design presented in this article has been performed at the IABG mbH of Ottobrunn, Germany, primarily intended for use in the new research flight

*Corresponding author: Technische Universität München, Institute of Flight System Dynamics, Boltzmannstraße 15, Garching D-85748, Germany. email: Florian.Holzapfel@tum.de

simulator of the Institute of Flight System Dynamics of the Technische Universität München in Munich, Germany.

2 REQUIREMENTS AND SPECIFICATIONS

As the primary purpose of the FCS design is to replicate the functional behaviour of a future transport aircraft, all announced and expected features for the configuration under consideration are to be implemented.

2.1 Functional specification

For pitch dynamics, the primary specifications are:

(a) a C* command law providing neutral flight-path stability from the pilot's point of view;
(b) scaling of the C* command to stay within the configuration-specific allowed load factor envelope at full stick deflections;
(c) an angle of attack command law at high angles of attack that prevents the aircraft from overshooting the angle of attack associated to the maximum lift coefficient;
(d) a speed command system for high speeds that allows speed control between maximum operating speed or Mach number and the maximum dive speed without overshooting the commanded value;
(e) a pitch angle limitation that restricts the steady-state pitch angle to a nominal range, allowing only mild and transient overshoots;
(f) positive pitch-stiffness during flare to provide natural behaviour during landing;
(g) turn compensation up to a certain bank angle;
(h) direct elevator and stabilizer control on the ground;
(i) a stabilizer auto-trim function continuously unloading the elevator using the stabilizer, to be frozen during landing, manoeuvring, or at the edge of the envelope;
(j) different degraded modes down to direct surface control supported by rudimentary damping feedbacks.

As far as lateral dynamics is concerned, the following requirements exist:

(a) stability axis roll rate control for normal bank angles with no sideslip excursions to be produced;
(b) direct bank angle control for higher bank angles with positive spiral stability up to a given limit bank angle;
(c) limitation of the maximum achievable steady-state bank angle allowing only small and transient overshoots;
(d) pedal commands angle of sideslip associated with a small build-up in bank angle;
(e) decoupling of roll and yaw axes in terms of disturbance response and attenuation;
(f) proper turn coordination;
(g) provision of a constant response behaviour over the whole envelope;
(h) positive spiral stability, i.e. direct bank angle control for all bank angles in phases where pitch axis protections are active;
(i) direct control surface control on the ground;
(j) different degraded modes down to direct aileron/roll-spoiler and rudder control augmented by rudimentary damping feedbacks.

2.2 Design and implementation requirements

Easy and quick adaptability to new aircraft datasets, different levels of model fidelity as well as fast modification of numeric values for handling qualities and limit values for the aircraft envelope are high-level requirements of paramount interest for the effort at hand. Thus, proper low-level requirements for the actual control design, implementation, and assessment have to be derived. These are as follows.

1. Parameterization of numeric handling qualities requirements and envelope protection and limitation values as a function of altitude (density), Mach number, and configuration parameters (mass, flaps, gear, and so on).
2. Implementation of automated gain and coefficient design routines for all laws and modes based on linearized plant models.
3. Implementation of automated assessment routines for linear analysis.
4. Implementation of routines to automatically generate regular table grid data from coefficients designed in available linearization points for gain scheduling.
5. Formulation of the gain design routines for dynamic systems of arbitrary order, i.e. not for rigid body approximations to account for sensor, sensor processing, and actuation system dynamics.
6. Modular implementation of the control system components and the mode switching logics, and minimization of interdependences.
7. Automated code-generation and build procedure for rapid prototyping.

From both the functional specification as well as from the design and implementation requirements presented above, detailed requirements concerning handling qualities, mode transitions, implementation and interfacing aspects, and so on have been derived. Military specifications, civilian certification standards as well as company proprietary software development and implementation processes complement the

proper formulation of the detailed problem statement and its solution process.

3 LATERAL-DIRECTIONAL CONTROL SYSTEM

3.1 Control system structure

The basic layout of the lateral-directional control system is depicted in Fig. 1. It can basically be broken down into four components, namely the command shaping and feed-forward path, the proportional integral feedback path, the control allocation, and the parallel path for the direct control law which is just augmented by rudimentary damping feedback.

The feedback portion consists of a full state feedback of the lateral-directional rigid body states, i.e. the stability axis roll rate p_S, the stability axis yaw rate r_S, the bank angle Φ, and an estimated angle of sideslip $\hat{\beta}$. The proportional feedback is performed by the 2×4 matrix $\mathbf{K}_P$. For the angle of sideslip, an estimate is used as flow angles are considered to be expensive feedback variables due to measurement noise and low measurement bandwidth if not filtered and augmented with inertial measurements. Additionally, integral feedback of the control errors in the bank angle and the angle of sideslip is performed as those two variables are the primary control variables of the inner loop of the lateral-directional control system, i.e. the inner loop is a bank angle, not a roll rate command system. It is to be noted that the integral feedback gain matrix is placed before the error integrators to increase the robustness in the non-linear implementation of the gain-scheduled control system.

The inputs to the integral error gain matrix consist of the errors between the commanded and the actual values of the bank angle and the angle of sideslip, respectively. The commanded values Φ_C and β_C are also multiplied by the feed forward matrix $\mathbf{H}_{\phi\beta}$, which is designed to cancel the integrator poles from the overall command input to output transfer function matrix.

Feed forward matrix, proportional feedbacks, and integral feedbacks are designed for decoupled control of bank angle and angle of sideslip as well as for steady-state accuracy in these two variables.

The three signal strings – feed forward, proportional feedback, and integral error feedback – are added up to two commanded virtual control variables, a virtual roll and yaw control command. Those virtual commands are transformed to physical control surface deflection commands in the control allocation

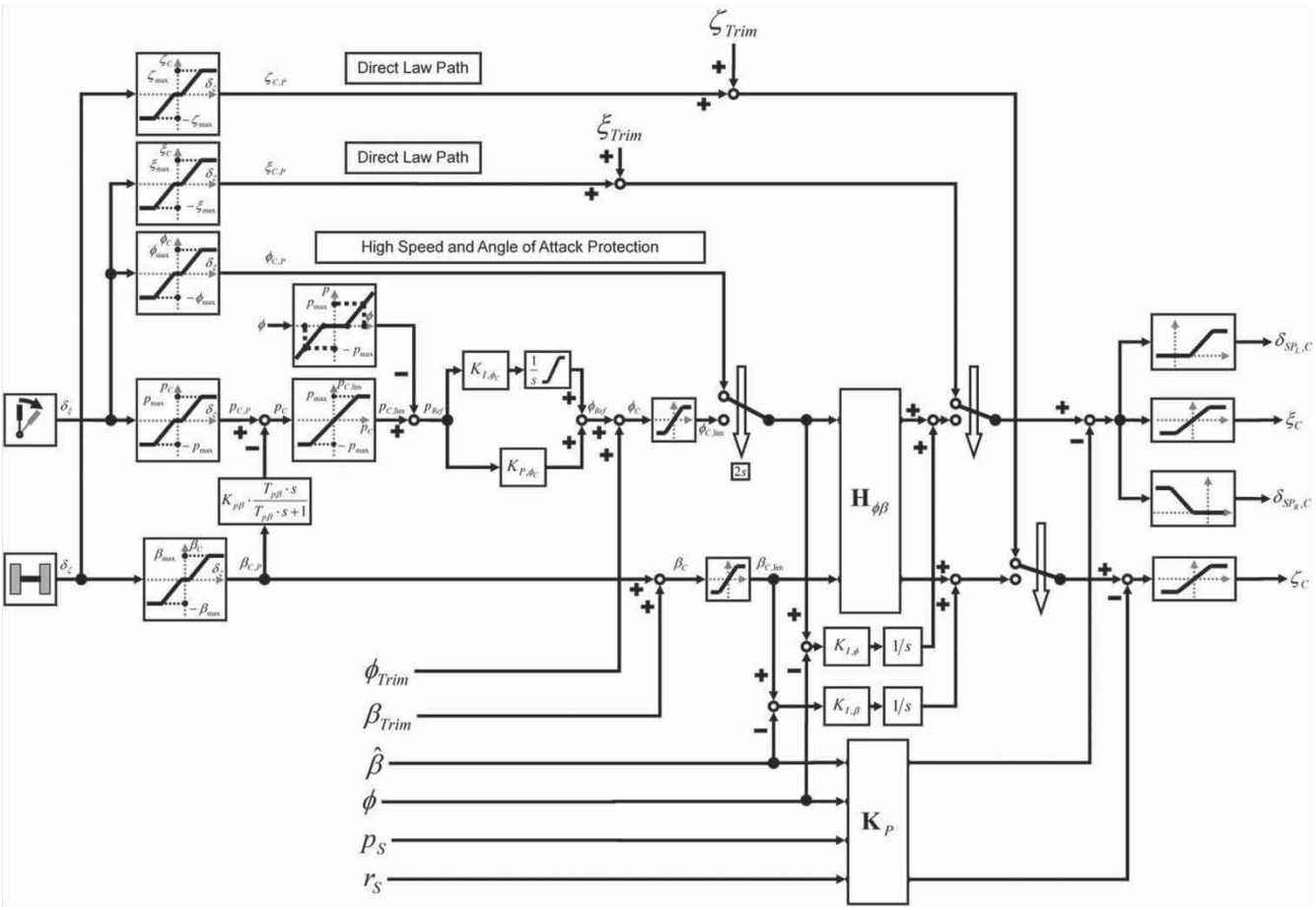

Fig. 1 Basic layout of the lateral-directional control system

portion, which forms the next element of the lateral control system.

The virtual roll control is designed to produce a pure stability axis rolling moment while the associated yawing moment vanishes; the yaw control produces the opposite effect. The transformation from virtual controls to physical commands for left and right ailerons, left and right asymmetric spoiler deflections as well as for the rudder is performed by flight condition-dependent look-up tables.

The third major part of the system is the command-shaping portion, generating the inner-loop commands for Φ_C and β_C from the two pilot inceptors for the lateral-directional dynamics, which are the lateral stick deflection δ_ξ and the pedal command δ_ζ. In the normal operating mode, the lateral stick command is scaled to produce the maximum design stability axis roll rate for a full deflection, whereas the pedal command is scaled to command the maximum design angle of sideslip when fully deflected. Both the maximum angle of sideslip and the maximum roll rate are scheduled over the dynamic pressure. The angle of sideslip command path is connected to the roll rate path via a high-pass filter. The purpose of this interconnection is to provide the natural buildup of a bank angle in conjunction with the commanded angle of sideslip as pilots are used to this behaviour from the inherent dynamics of an uncontrolled aircraft. This characteristic must be actively added as the inner loop of the lateral control system decouples the roll and the yaw axes so that the bank angle would remain zero during the buildup of a commanded angle of sideslip.

As the superimposed roll rate command from the lateral stick and the high-pass filtered pedal cross feed could exceed the maximum design roll rate, the total roll rate command is limited again to the allowed limit rate.

Adding a bank angle-dependent roll rate to the pilot-commanded roll rate implements both positive spiral stability when a certain bank angle is exceeded and a limitation of the absolute bank angle [**1**]. This is achieved by a linear increase of $p_C(\Phi)$ from zero at the bank angle at which positive spiral stability is to begin to the negative amount of the maximum allowed roll rate at the limit design bank angle Φ_{lim}, fully cancelling the roll rate commanded by the pilot and thus not allowing him to increase the bank angle over the limit value.

To this point, the lateral stick command is still interpreted as a roll rate, whereas the inner loop was presented as a bank angle command system. Thus, a PI command filter is used to transform the pilot roll rate command to a desired bank angle [**2**]. The zero of the command filter cancels the stable spiral pole, while the filter pole is located in the origin of the complex plane. This provides the pilot with the desired neutral spiral stability behaviour for bank angles below the threshold value for positive spiral stability whereas the inner loop features strong spiral stability, thus tracking the commanded bank angle with steady-state accuracy and countering external disturbances.

For zero cockpit control deflections and small values of the PI filter integrator below a specified threshold bank angle, the integrator is reset to zero to assist wings-level flight. The integrator reset is immediately stopped for non-zero roll rate command to allow the pilot to actively control small bank angles.

At this point, steady trim values are added to the commanded bank angle and the commanded angle of sideslip, which can be used to produce offsets from zero for centred controls, e.g. to counter asymmetries. As the sum of the pilot command and the trim provided reference value may exceed the allowed limit values, a last command limiting is performed. In case one of the hard pitch dynamics protections, either the angle of attack or the high-speed protection, is active, the bank angle command generated as described above is replaced by a bank angle that is proportional to the lateral stick deflection. This leads to positive spiral stability in the stick to bank angle transfer function for all bank angles, replacing the roll rate command by a direct bank angle command. Switching between the two alternative bank angle command sources is performed by linear blending over 2 s upon activation or deactivation of one of the relevant pitch dynamics protections.

Finally, the fourth part of the lateral directional control system consists of the direct command law bypassing the whole command filter. In this case, the lateral stick and the pedal deflections are directly scaled to deflections of the virtual roll and yaw control, augmented by a trim value, which replicates conventional aileron or rudder trim to achieve steady-state control surface deflections with centred pilot inceptors. If the direct law is active, those defections are fed to the control allocation section with just proportional roll rate feedback added to the roll command and proportional yaw rate feedback added to the yaw command. All other proportional feedbacks as well as the integral feedbacks and the whole command shaping and feed forward portion of the normal command law are deactivated in this mode.

3.2 Control system design

With the functional structure of the lateral-directional control system illuminated, focus is now on the determination of the available coefficients – the feedback and filter gains, filter coefficients, and feed forwards.

The most important numeric requirements for the lateral-directional control system that have been selected for the control design at hand are as follows:

(a) dutch roll damping and natural frequency: $1/2 \cdot \sqrt{2}$ and 2 rad/s;

(b) roll subsidence mode time constant T_R: selected to be very fast;
(c) spiral mode time constant T_S: two different philosophies have been pursued – stable and slow and stable and very fast;
(d) integrator poles: both selected to be fast – $s_{I,\beta} = -1$ and $s_{I,\phi} = -0.7$;
(e) modal decoupling: amplitude ratio $|\phi/\beta|$ in the dutch roll eigenvector to be set to zero;
(f) roll response criterion $T_{\phi=45^\circ}$ set to a rather crisp value;
(g) steady-state ratio for bank angle command induced by angle of sideslip command: $\phi_{SS}/\beta_{SS} = -1.5$;
(h) stability requirements: amplitude margin $A_R = 6$ dB, phase margin $\phi_R = 45^\circ$ for both roll and yaw loop cut (cut performed at the virtual controls);
(i) stability and robustness to be monitored and increased using the smallest singular value of the feedback difference function and the conditioning index $\vec{\sigma}/\underline{\sigma}$ of the closed-loop system matrix.

The items detailed above automatically ensure compliance with other requirements. The modal decoupling eliminates all questions concerning proverse or adverse yaw characteristics or sideslip excursions from roll inputs. The high dutch roll damping also ensures compliance with roll rate and bank angle oscillation requirements.

For the computation of feedback gains, eigenstructure assignment is to be used [**2**–**6**]. The selected eigenstructure is summarized in Fig. 2. The desired eigenvalues are set to the values detailed above. For the eigenvectors, the following selections are made with the aim of decoupling the roll and the yaw axes.

1. The roll rate and the bank angle entry in the dutch roll eigenvectors are set to zero.
2. The yaw rate and the angle of sideslip entries in the eigenvectors of the roll subsidence mode and the spiral mode are set to zero.

		Dutch Roll	Spiral Mode	Roll Mode	ϕ Integral	β Integral
		$\omega_{0,RG} = 2\,rad/s$ $\zeta_{RG} = 0.5 \cdot \sqrt{2}$	$T_S = 2s$ $\lambda_S = -0.5s^{-1}$	$T_R = 0.7s$ $\lambda_R = -1.4s^{-1}$	$\lambda_{I_\phi} = -0.5s^{-1}$	$\lambda_{I_\beta} = -1s^{-1}$
Eigenvector Components	p	**0**				
	ϕ	**0**				
	r		**0**	**0**		
	β		**0**	**0**		
	ϕ_I				**1**	**0**
	β_I				**0**	**1**
	$\hat{\beta}$					
	ξ					
	$\dot{\xi}$					
	ζ					
	$\dot{\zeta}$					
	δ_S					
	$\dot{\delta}_S$					

Fig. 2 Selected eigenstructure for the lateral-directional control system

3. For the integrator modes, the bank angle entry in the eigenvector for the bank angle mode is set to one, whereas the angle of sideslip entry is set to zero. For the angle of sideslip mode, the opposite procedure is performed.
4. As only two controls are available, namely the virtual roll and yaw commands, only two eigenvector elements may be specified. Thus the entries of the eigenvectors not mentioned above are marked as non-relevant so that the degrees of freedom available for influencing the eigenvectors are not wasted for unimportant elements.

To correctly place the closed-loop system poles and shape the eigenvectors, it is not sufficient to perform the design process for the rigid-body lateral dynamics alone. The assignment procedure is applied to the full system augmented by the error integrators $x_{I,\beta}, x_{I,\Phi}$ and second-order models for aileron $x_\xi, x_{\dot{\xi}}$, roll-spoiler $x_\zeta, x_{\dot{\zeta}}$, and rudder actuators $x_{\delta_S}, x_{\dot{\delta}_S}$. This leads to a linear system represented by the linear state space model of the plant augmented by the two integrators and the actuator states

$$\dot{\boldsymbol{x}} = \mathbf{A}\boldsymbol{x} + \mathbf{B}\boldsymbol{u} \tag{1}$$

The control variables are the virtual roll and yaw commands $\delta_{\text{Roll,cmd}}$ and $\delta_{\text{Yaw,cmd}}$

$$\boldsymbol{u} = [\delta_{\text{Roll,cmd}}, \delta_{\text{Yaw,cmd}}]^T$$

The state vector contains the stability axes yaw and roll rates r_S and p_S, the angle of sideslip β, and the bank angle Φ as rigid body states, the states x_ξ, $x_{\dot{\xi}}$, x_ζ, $x_{\dot{\zeta}}$, x_{δ_S}, $x_{\dot{\delta}_S}$ as deflection and rate states of the linear second-order actuator models, and the control system states $x_{I,\beta}$ and $x_{I,\Phi}$ representing the integrators to provide steady-state accuracy in Φ and β

$$x = [r_S, \beta, p_S, \Phi, x_\xi, x_{\dot{\xi}}, x_\zeta, x_{\dot{\zeta}}, x_{\delta_S}, x_{\dot{\delta}_S}, x_{I,\beta_K}, x_{I,\Phi}]^T$$

It should be mentioned that the linear system may be extended by further states, e.g. sensor, sensor filtering or processing states, elastic modes, and so on, without limiting or restricting the applicability of the implemented procedure.

Since not all states are available for feedback, the system has to be designed by means of output feedback. The outputs collected in the output vector $\boldsymbol{y}$ are composed of r_S and p_S computed from the body-axes rates p and r, the bank angle Φ available from direct IMU measurement, the estimated angle of sideslip $\hat{\beta}$, and the known control system states $x_{I,\beta}$ and $x_{I,\Phi}$. In the linear model, the outputs are computed from the states according to

$$\boldsymbol{y} = \mathbf{C}\boldsymbol{x} \tag{2}$$

To sum up, the linear system features $n = 12$ states, $m = 2$ inputs, and $r = 8$ outputs. The output feedback can be formulated as

$$\boldsymbol{u} = -\mathbf{K}\boldsymbol{y} + \boldsymbol{u}_{\mathrm{C}} \tag{3}$$

leading to the closed-loop dynamics

$$\dot{\boldsymbol{x}} = \underbrace{(\mathbf{A} - \mathbf{BKC})}_{\tilde{\mathbf{A}}} \cdot \boldsymbol{x} + \mathbf{B} \cdot \boldsymbol{u}_{\mathrm{C}} \tag{4}$$

where the aim of the control design is to determine the gain matrix $\mathbf{K}$ to give the closed-loop system the desired dynamics $\tilde{\mathbf{A}}$, which is composed of the eigenvalues and eigenvectors detailed at the beginning of this article.

The closed-loop eigenvalues λ_i and eigenvectors $\boldsymbol{v}_i$ are determined by the equation

$$(\mathbf{A} - \mathbf{BKC}) \cdot \boldsymbol{v}_i = \boldsymbol{v}_i \cdot \lambda_i \tag{5}$$

This equation can be restructured to yield

$$\begin{bmatrix} \lambda_i \boldsymbol{I} - \mathbf{A} & \mathbf{B} \end{bmatrix} \cdot \begin{bmatrix} \boldsymbol{v}_i \\ \mathbf{KC}\boldsymbol{v}_i \end{bmatrix} = \begin{bmatrix} \lambda_i I - \mathbf{A} & \mathbf{B} \end{bmatrix} \cdot \begin{bmatrix} \boldsymbol{v}_i \\ \boldsymbol{z}_i \end{bmatrix} = \mathbf{0} \tag{6}$$

with $\boldsymbol{z}_i = \mathbf{KC}\boldsymbol{v}_i$ being the so-called input directions. Any non-trivial solution $\begin{bmatrix} \boldsymbol{v}_i^{\mathrm{T}} & \boldsymbol{z}_i^{\mathrm{T}} \end{bmatrix}^{\mathrm{T}}$ of this linear equation system must be within the kernel of the matrix $\begin{bmatrix} \lambda_i \boldsymbol{I} - \mathbf{A} & \mathbf{B} \end{bmatrix}$, i.e.

$$\begin{bmatrix} \boldsymbol{v}_i \\ \boldsymbol{z}_i \end{bmatrix} \in \mathrm{Ker} \left\{ \begin{bmatrix} \lambda_i \boldsymbol{I} - \mathbf{A} & \mathbf{B} \end{bmatrix}_{n \times (n+m)} \right\} \tag{7}$$

For the chosen closed-loop eigenvalues, it is important that there are no eigenvalues of the open-loop system, i.e. that $\lambda_i \boldsymbol{I} - \mathbf{A}$ is of full rank

$$\mathrm{rank}\{\lambda_i \boldsymbol{I} - \mathbf{A}\} = n \tag{8}$$

In that case, any possible solution of the described linear equation (6) can be formulated as an arbitrary combination of the basis vectors of the nullspace $\overline{\mathbf{N}}_{\lambda_i}$ of the matrix $\begin{bmatrix} \lambda_i \boldsymbol{I} - \mathbf{A} & \mathbf{B} \end{bmatrix}$

$$\begin{aligned} (\overline{\boldsymbol{n}}_1)_{(m+n)\times 1} &= \begin{bmatrix} (n_1)_{n\times 1} \\ (\hat{n}_1)_{m\times 1} \end{bmatrix}, \ldots, \quad \overline{\boldsymbol{n}}_m = \begin{bmatrix} \boldsymbol{n}_m \\ \hat{\boldsymbol{n}}_m \end{bmatrix} \\ \overline{\mathbf{N}}_{\lambda_i} &= \begin{bmatrix} \overline{\boldsymbol{n}}_{1,\lambda_i} & \cdots & \overline{\boldsymbol{n}}_{m,\lambda_i} \end{bmatrix} = \begin{bmatrix} \boldsymbol{n}_{1,\lambda_i} & \cdots & \boldsymbol{n}_{m,\lambda_i} \\ \hat{\boldsymbol{n}}_{1,\lambda_i} & \cdots & \hat{\boldsymbol{n}}_{m,\lambda_i} \end{bmatrix} \\ &= \begin{bmatrix} \mathbf{N}_{\lambda_i} \\ \hat{\mathbf{N}}_{\lambda_i} \end{bmatrix} \end{aligned} \tag{9}$$

where the base vectors $\overline{\boldsymbol{n}}_i$ of the nullspace can be separated into the upper part $\boldsymbol{n}_i$ related to the eigenvector and the lower part $\hat{\boldsymbol{n}}_i$ related to the corresponding input direction. This leads to the following expression for the achievable eigenvalues and eigenvectors

$$\begin{bmatrix} \boldsymbol{v}_i \\ \boldsymbol{z}_i \end{bmatrix} = \begin{bmatrix} \overline{\boldsymbol{n}}_{1,\lambda_i} & \cdots & \overline{\boldsymbol{n}}_{m,\lambda_i} \end{bmatrix} \cdot \begin{bmatrix} l_{1,\lambda_i} \\ \vdots \\ l_{m,\lambda_i} \end{bmatrix} \overline{\mathbf{N}}_{\lambda_i} \cdot l_{\lambda_i} = \begin{bmatrix} \mathbf{N}_{\lambda_i} \\ \hat{\mathbf{N}}_{\lambda_i} \end{bmatrix} \cdot l_{\lambda_i} \tag{10}$$

or in separate equations $\boldsymbol{v}_i = \mathbf{N}_{\lambda_i} \cdot l_{\lambda_i}$ and $\boldsymbol{z}_i = \hat{\mathbf{N}}_{\lambda_i} \cdot l_{\lambda_i}$, with $l_{\lambda_i} = \begin{bmatrix} l_{1,\lambda_i} & \cdots & l_{m,\lambda_i} \end{bmatrix}^{\mathrm{T}}$ being an arbitrary parameter vector.

As already mentioned, the number of elements per eigenvector that may be specified during the design is equal to the number m of controls available. As not all elements of the eigenvector are of equal importance to the design, sorting matrices $(\mathbf{P}_i^{\mathrm{S}})_{s\times n}$ and $(\mathbf{P}_i^{\mathrm{U}})_{(n-s)\times ni}$ are introduced for every eigenvector/eigenvalue combination, collecting the elements of interest, i.e. those to be specified (S) in the upper rows and those that are not of interest, i.e. those that may remain unspecified (U) in the lower lines

$$\begin{bmatrix} (\boldsymbol{v}_i^{\mathrm{S}})_{s\times 1} \\ (\boldsymbol{v}_i^{\mathrm{U}})_{(n-s)\times 1} \end{bmatrix} = \begin{bmatrix} (\mathbf{P}_i^{\mathrm{S}})_{s\times n} \\ (\mathbf{P}_i^{\mathrm{U}})_{(n-s)\times n} \end{bmatrix} \cdot \boldsymbol{v}_i \tag{11}$$

The sorting matrices feature only one non-zero entry per line or column which features a value of one. The sorting matrix for the specified elements is also used to extract the relevant entries from the eigenvector-related part of the basis of the nullspace

$$\mathbf{N}_{\lambda_i}^{\mathrm{S}} = \mathbf{P}_i^{\mathrm{S}} \cdot \mathbf{N}_{\lambda_i} \tag{12}$$

For the elements to be specified, the desired values are defined in the design eigenvector $\boldsymbol{v}_{\mathrm{id}}^{\mathrm{S}}$. If more elements are to be specified than possible (i.e. more than m elements), the desired eigenvector cannot be achieved perfectly. Thus the user may add a positive definite weighting matrix $\mathbf{Q}_{\lambda_i}$ for every eigenvector/eigenvalue combination that specifies which elements are of higher and lower importance. By means of this matrix, the weighted desired eigenvectors $\overline{\boldsymbol{v}}_{\mathrm{id}}^{\mathrm{S}}$ can be computed

$$\overline{\boldsymbol{v}}_{\mathrm{id}}^{\mathrm{S}} = \mathbf{Q}_{\lambda_i} \cdot \boldsymbol{v}_{\mathrm{id}}^{\mathrm{S}} \tag{13}$$

Putting together the above-stated equations, the desired values for the specified entries of the eigenvectors $\boldsymbol{v}_{\mathrm{id}}^{\mathrm{S}}$ are connected to the parameter vector $\boldsymbol{l}_{\lambda_i}$

$$\overline{\boldsymbol{v}}_{\mathrm{id}}^{\mathrm{S}} = \mathbf{Q}_{\lambda_i} \cdot \boldsymbol{v}_{\mathrm{id}}^{\mathrm{S}} = \mathbf{Q}_{\lambda_i} \cdot \mathbf{P}_i^{\mathrm{S}} \cdot \mathbf{N}_{\lambda_i} \cdot \boldsymbol{l}_{\lambda_i} = \mathbf{Q}_{\lambda_i} \cdot \mathbf{N}_{\lambda_i}^{\mathrm{S}} \cdot \boldsymbol{l}_{\lambda_i} \tag{14}$$

The results are eigenvector elements that fit best in terms of weighted least squares minimization.

If the number of specified elements is larger than the number of controls available, this equation features the dimensions

$$(\mathbf{Q}_{\lambda_i})_{s\times s}\cdot(\boldsymbol{v}^{\mathrm{S}}_{\mathrm{id}})_{s\times 1}=(\mathbf{Q}_{\lambda_i})_{s\times s}\cdot(\mathbf{N}^{\mathrm{S}}_{\lambda_i})_{s\times m}\cdot(\boldsymbol{l}_{\lambda_i})_{m\times 1} \tag{15}$$

As expected, with the matrix $(\mathbf{Q}_{\lambda_i})_{s\times s}\cdot(\mathbf{N}^{\mathrm{S}}_{\lambda_i})_{s\times m}$ on the right-hand side not being square, the equation cannot be explicitly solved for $\boldsymbol{l}_{\lambda_i}$. Thus, a pseudo-inverse approach is chosen

$$\mathbf{l}_{\lambda_i}=[(\mathbf{N}^{S}_{\lambda_i})^{H}\cdot\mathbf{Q}_{\lambda_i}\cdot\mathbf{N}^{S}_{\lambda_i}]^{-1}\cdot(\mathbf{N}^{S}_{\lambda_i})^{H}\cdot\mathbf{Q}_{\lambda_i}\cdot\mathbf{v}^{S}_{id} \tag{16}$$

If the number of eigenvector elements to be specified is equal to the number of control effectors available, the equation yields the dimensions

$$(\mathbf{Q}_{\lambda_i})_{m\times m}\cdot(\boldsymbol{v}^{\mathrm{S}}_{\mathrm{id}})_{m\times 1}=[(\mathbf{Q}_{\lambda_i})_{m\times m}\cdot(\mathbf{N}^{\mathrm{S}}_{\lambda_i})_{m\times m}]\cdot(\boldsymbol{l}_{\lambda_i})_{m\times 1} \tag{17}$$

and thus may be directly solved for the parameter vector

$$\boldsymbol{l}_{\lambda_i}=[\mathbf{Q}_{\lambda_i}\cdot\mathbf{N}^{\mathrm{S}}_{\lambda_i}]^{-1}\cdot\mathbf{Q}_{\lambda_i}\cdot\boldsymbol{v}^{\mathrm{S}}_{\mathrm{id}}\quad\text{i.e. }\boldsymbol{l}_{\lambda_i}=(\mathbf{N}^{\mathrm{S}}_{\lambda_i})^{-1}\cdot\boldsymbol{v}^{\mathrm{S}}_{\mathrm{id}} \tag{18}$$

This is not performed by inverting the matrix $\mathbf{N}^{\mathrm{S}}_{\lambda_i}$, but by QR-decomposition-based linear equation solving.

With the parameter vector $\boldsymbol{l}_{\lambda_i}$ for the best possible approximation of the desired eigenvector (i.e. the projection of the desired eigenvector into the nullspace spanning the space of achievable eigenvectors) now known, the achievable eigenvector $\boldsymbol{v}_i$ and the corresponding input direction $\boldsymbol{z}_i$ can be computed

$$\boldsymbol{v}_i=\mathbf{N}_{\lambda_i}\cdot\boldsymbol{l}_{\lambda_i},\quad \boldsymbol{z}_i=\hat{\mathbf{N}}_{\lambda_i}\cdot\boldsymbol{l}_{\lambda_i}, \tag{19}$$

Using the definition of the input directions, $\boldsymbol{z}_i=\mathbf{K}\cdot\mathbf{C}\cdot\boldsymbol{v}_i$, these equations can now be used to calculate the gain matrix $\mathbf{K}$. As

$$\begin{bmatrix}\boldsymbol{z}_1 & \boldsymbol{z}_r & \cdots & \boldsymbol{z}_r\end{bmatrix}_{m\times r}=\mathbf{K}_{m\times r}\cdot\mathbf{C}_{r\times n}\cdot\begin{bmatrix}\boldsymbol{v}_1 & \boldsymbol{v}_2 & \cdots & \boldsymbol{v}_r\end{bmatrix}_{n\times r} \tag{20}$$

the result is

$$\mathbf{K}=\begin{bmatrix}\boldsymbol{z}_1 & \boldsymbol{z}_2 & \cdots & \boldsymbol{z}_r\end{bmatrix}\cdot\left(\mathbf{C}\cdot\begin{bmatrix}\boldsymbol{v}_1 & \boldsymbol{v}_2 & \cdots & \boldsymbol{v}_r\end{bmatrix}\right)^{-1} \tag{21}$$

As far as the control allocation algorithm is concerned, the distribution from virtual roll and yaw controls, used as the only two independent controls for the eigenstructure assignment, to physical surface deflections is computed based on weighted generalized pseudo-inverses. If the commanded physical control vector consisting of aileron, roll spoiler, and rudder deflections is $\boldsymbol{u}_{\mathrm{lat}}$ while the virtual control vector is $\overline{\boldsymbol{u}}_{\mathrm{lat}}$, then the allocation matrix $\mathbf{K}_{\mathrm{Alloc,lat}}$ mapping $\overline{\boldsymbol{u}}_{\mathrm{lat}}$ to $\boldsymbol{u}_{\mathrm{lat}}$ by $\boldsymbol{u}_{\mathrm{lat}}=\mathbf{K}_{\mathrm{Alloc,lat}}\cdot\overline{\boldsymbol{u}}_{\mathrm{lat}}$ has to satisfy

$$\begin{bmatrix}L_\xi & L_\zeta & L_{\delta_S}\\ N_\xi & N_\zeta & N_{\delta_S}\end{bmatrix}\cdot\mathbf{K}_{\mathrm{Alloc,lat}}=\begin{bmatrix}1 & 0\\ 0 & 1\end{bmatrix} \tag{22}$$

As this equation features an infinite number of solutions, the use of the three control surfaces can be relatively weighted by a 3×3 positive definite weighting matrix $\mathbf{W}_{\mathrm{Alloc,lat}}$, where higher values stand for increasing the utilization of the corresponding control surface.

The resulting control allocation matrix is determined using

$$\mathbf{K}_{\mathrm{Alloc,lat}}=\mathbf{W}^{-1}_{\mathrm{Alloc,lat}}\cdot\mathbf{B}^{\mathrm{T}}_{\mathrm{lat}}\cdot(\mathbf{B}_{\mathrm{lat}}\cdot\mathbf{W}^{-1}_{\mathrm{Alloc,lat}}\cdot\mathbf{B}^{\mathrm{T}}_{\mathrm{lat}}) \tag{23}$$

If moment demands cannot be produced by the allocation scheme provided by $\mathbf{K}_{\mathrm{Alloc,lat}}$ as control surfaces start to saturate, the remaining moment demand is redistributed to the non-saturated surfaces. In this case however, the decoupling property of the controls is lost.

The feed forward matrix $\mathbf{H}_{\phi\beta}$ is computed to cancel the two poles introduced by the error integrators; hence those are not visible in the stick/pedal to bank/sideslip transfer functions.

In the PI bank angle command filter, the integral gain is set to one and the transfer function zero is placed to cancel the stable spiral mode of the inner loop producing neutral spiral stability in the stick to bank transfer function when the absolute bank angle is below the threshold value. A detailed description of the lateral-directional control system can be taken from reference [7].

3.3 Stability and robustness

So far, the desired eigenvalues of the closed-loop system have been assigned exactly and the eigenvectors in the best possible way.

Now, an extension to the approach is introduced that increases the robustness of the closed-loop system. As a trade-off, the demand to exactly achieve the desired eigenvalues has to be relaxed as well as the requirement to approximate the desired eigenvector in the best achievable way.

To consider robustness against parameter uncertainties, the schematic representation of the closed-loop system as depicted in Fig. 3 is considered. The system containing the controller and the plant has been augmented by a diagonal matrix containing unstructured uncertainties

$$\mathbf{\Delta}=\mathrm{diag}\,\{\Delta_1,\ldots,\Delta_m\}\quad\text{with }\Delta_l=r_l\cdot e^{i\phi_l} \tag{24}$$

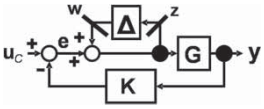

Fig. 3 Consideration of uncertainties in the control loop

The transfer function from the output of the uncertainty block to its input is

$$z = [\boldsymbol{I} + \mathbf{K} \cdot \mathbf{G}]^{-1} \cdot \mathbf{w} = \mathbf{S} \cdot \mathbf{w} \tag{25}$$

where **S** is the sensitivity function matrix. According to the small gain theorem, robust stability is guaranteed for the perturbed system as long as for the smallest signal value $\underline{\sigma}$ and for the largest signal value $\overline{\sigma}$

$$\overline{\sigma}(\mathbf{\Delta}) \cdot \overline{\sigma}(\mathbf{S}) < 1$$

with

$$\overline{\sigma}(\mathbf{S}) = \frac{1}{\underline{\sigma}(\mathbf{S}^{-1})} = \frac{1}{\underline{\sigma}(\mathbf{F})} \tag{26}$$

where **F** is the feedback difference function matrix at the actuator inputs

$$\mathbf{F}(s) = \mathbf{I} + \mathbf{K} \cdot \mathbf{G}(s) \tag{27}$$

This leads to the inequality

$$\overline{\sigma}(\mathbf{\Delta}) < \underline{\sigma}(\mathbf{F}) \tag{28}$$

As **F** is a frequency-dependent function matrix, robust stability is only ensured if

$$\overline{\sigma}(\mathbf{\Delta}) < r_{\min} = \inf_{\omega \in R} \underline{\sigma}[\mathbf{F}(j\omega)] \tag{29}$$

In an effort to increase system robustness, the question is how the desired eigenvalues may be modified mildly within bounds to increase $r_{\min}$. This may be achieved by means of an iterative gradient-based procedure. The desired eigenvalues are collected as $\boldsymbol{p}_{\mathrm{d}} = \begin{bmatrix} T_{\mathrm{S,d}} & T_{\mathrm{R,d}} & \zeta_{\mathrm{RG,d}} & \omega_{n,\mathrm{RG,d}} \end{bmatrix}^{\mathrm{T}}$, whereas the perturbed eigenvalues are put into the vector $\boldsymbol{p} = \begin{bmatrix} T_{\mathrm{S}} & T_{\mathrm{R}} & \zeta_{\mathrm{RG}} & \omega_{n,\mathrm{RG}} \end{bmatrix}^{\mathrm{T}}$.

Increasing the robustness of the system by limited perturbations of the desired eigenvalues is equivalent to minimizing the cost function

$$E = -\frac{1}{2} \cdot w_r \cdot r_{\min}^2 + \frac{1}{2} (\boldsymbol{p} - \boldsymbol{p}_{\mathrm{d}})^{\mathrm{T}} \cdot \mathbf{W}_{\mathrm{p}} \cdot (\boldsymbol{p} - \boldsymbol{p}_{\mathrm{d}}) \tag{30}$$

Thus, the cost function can be successively reduced by the reduction step

$$\Delta \boldsymbol{p} = -\eta \cdot \frac{\partial E}{\partial \boldsymbol{p}} \tag{31}$$

The gradient $\partial E / \partial \boldsymbol{p}$ of the cost function is computed according to

$$\frac{\partial E}{\partial \boldsymbol{p}} = -w_r \cdot r_{\min} \cdot \frac{\partial r_{\min}}{\partial \boldsymbol{p}} + \mathbf{W}_{\mathrm{p}} \cdot (\boldsymbol{p} - \boldsymbol{p}_{\mathrm{d}}) \tag{32}$$

where the gradient of $r_{\min}$

$$\frac{\partial r_{\min}}{\partial \boldsymbol{p}} = \begin{bmatrix} \frac{\partial r_{\min}}{\partial T_{\mathrm{S}}} & \frac{\partial r_{\min}}{\partial T_{\mathrm{R}}} & \frac{\partial r_{\min}}{\partial \zeta_{\mathrm{RG}}} & \frac{\partial r_{\min}}{\partial \omega_{n,\mathrm{RG}}} \end{bmatrix}^{\mathrm{T}} \tag{33}$$

is computed by numerical differentiation.

With the following relation, it can be verified that applying $\Delta \boldsymbol{p}$ leads to a reduction of the cost function

$$\Delta E = -\eta \cdot \left[-w_r \cdot r_{\min} \cdot \frac{\partial r_{\min}}{\partial \boldsymbol{p}} + \mathbf{W}_{\mathrm{p}} \cdot (\boldsymbol{p} - \boldsymbol{p}_{\mathrm{d}}) \right]^2 \leqslant 0 \tag{34}$$

As far as the eigenvectors are concerned, they can also be iteratively modified to increase the robustness of the closed-loop system. This is achieved by continuous orthogonalization of the eigenvectors. For every eigenvector to be assigned, the direction of the desired eigenvector is adjusted by projecting it on a vector that is perpendicular to all other eigenvectors. Orthogonalization increases system robustness by improving the condition number of the modal matrix reducing mode interactions.

4 PITCH AXIS CONTROL SYSTEM

The basic layout of the pitch axis control system is depicted in Fig. 4. This portion of the system features multiple limitation and protection modes requiring transient free blending.

4.1 Normal operating law

The command input to the inner loop core is a stability frame normal load factor increment $\Delta n_{Z,\mathrm{S}}$ to the current trim condition that is represented by linear flight trajectory at a given flight-path angle γ and flight-path bank angle μ. The intention of the pitch axis control system is to provide neutral flight-path stability, i.e. for zero stick deflection, the aircraft keeps the flight path in the vertical plane as the trim load factor of $n_{Z,\mathrm{Trim}} = \cos\gamma \cdot \cos\mu$ is maintained.

In normal operation, the inner loop of the longitudinal FCS portion controls the stability frame normal load factor increment $\Delta n_{Z,\mathrm{S}}$, which is the stability axis load factor $n_{Z,\mathrm{S}}$ corrected for the trim contribution of the current flight condition

$$\Delta n_{Z,\mathrm{S}} = n_{Z,\mathrm{S}} - n_{Z,\mathrm{Trim}} \tag{35}$$

To accomplish that, the pitch rate q and the normal load factor increment $\Delta n_{Z,\mathrm{S}}$ are used in proportional

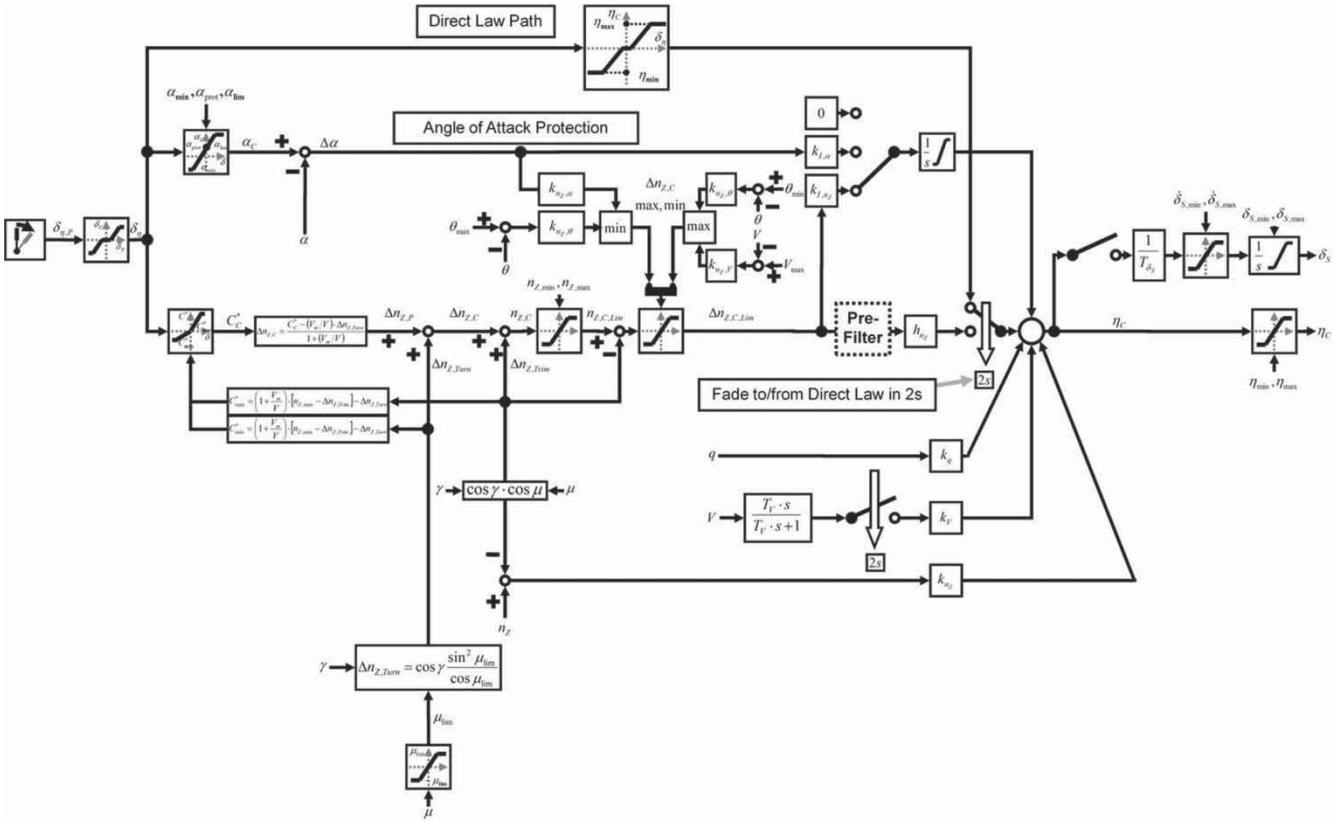

Fig. 4 Basic layout of the pitch control system

feedbacks with gains k_q and k_{n_Z}. An additional integral feedback is applied to the control error in the normal load factor increment with the feedback gain k_{I,n_Z} to provide steady-state accuracy. The feedback gains are designed to produce a short period mode with damping $\zeta_{SP} = 0.7$ and a natural frequency $\omega_{n,SP}$ corresponding to a control anticipation parameter (CAP) of one. The pole of the $\Delta n_{Z,S}$ integrator is selected to be very fast, which yields the advantage of rapidly producing a trim elevator deflection associated with the commanded flight condition. The three desired poles are exactly designed by applying pole placement to the complete linear system using the independent measurement of the pitch rate q and the stability axis normal load factor increment $\Delta n_{Z,S}$ and the known value of the controller state of the load factor integrator x_{I,n_Z}.

The feed forward gain $h_{n_Z} = -k_{I,n_Z}/s_{I,n_Z}$ is selected to cancel the error integrator pole from the stick to load factor transfer function, efficiently hiding the integrator dynamics from the pilot, which otherwise would lead to unnatural and therefore undesirable behaviour for him.

The commanded input signal to the inner loop, the load factor increment $\Delta n_{Z,S}$, is generated by the command shaping path. In normal flight, the pilot is required to command C* defined as

$$C^* = \Delta n_{z,s} + \left(\frac{V_m}{g}\right) \cdot q \tag{36}$$

This accounts for the fact that for small speeds the pitch rate gets more attention whereas at higher speeds the focus is on the load factor. The speed V_m is the so-called cross-over velocity, concerning weighting between pitch rate q and load factor $\Delta n_{Z,S}$ contribution to C*.

The pilot commands C* in normal flight whereas the inner loop controls the load factor. Accordingly, the pitch stick input must be shaped in a way that full forward and aft deflections always correspond to the absolute limit values for the normal load factor which is allowed for the current flight condition and configuration (considering gear, flap position, and so on.). Thus, the normalized stick command is linearly scaled from $[-1, 0, 1]$ to $[C^*_{min}, 0, C^*_{max}]$ using

$$C^*_{min\,/\,max} = \left(1 + \frac{V_m}{V}\right) \cdot (n_{Z,min\,/\,max} - n_{Z,Trim}) - \Delta n_{Z,Turn} \tag{37}$$

which is based on the quasi-steady-state relationship between linear system load factor and pitch rate response. The load factor increment $\Delta n_{Z,Turn}$ later added to the command signal has to be considered with regard to stick input scaling to avoid null-zones at the bounds of the stick travel.

Then, the pilot C* command is converted into an equivalent $\Delta n_{Z,\mathrm{S}}$ pilot command using the relation

$$\Delta n_{Z,\mathrm{S,C,Pilot}} = \frac{\mathrm{C}^*}{(1 + V_m/V)} \tag{38}$$

The total commanded load factor difference

$$\Delta n_{Z,\mathrm{S,C}} = \Delta n_{Z,\mathrm{S,C,Pilot}} + \Delta n_{Z,\mathrm{Turn}} \tag{39}$$

also includes the turn compensation component $\Delta n_{Z,\mathrm{Turn}}$, which compensates the rotation of the lift vector out of the horizontal plane up to a certain flight-path bank angle, eliminating the need for the pilot to apply additional back pressure on the pitch control to maintain the current flight-path angle.

As structural limitations do not apply to load factor increments but to the absolute value of the normal load factor $n_{Z,\mathrm{Trim}}$, the resulting command value for the absolute normal load factor also containing the trim load factor $n_{Z,\mathrm{Trim}}$ must be computed before command limiting can be performed

$$n_{Z,\mathrm{S,C}} = \Delta n_{Z,\mathrm{S,C,Pilot}} + \Delta n_{Z,\mathrm{Turn}} + n_{Z,\mathrm{Trim}} \tag{40}$$

This value is clipped to account for the configuration-dependent load factor limitations of the aircraft. After that, the trim value is deducted again to produce the now limited command value $\Delta n_{Z,\mathrm{S,C,Lim}}$ required as command input for the inner loop.

For further processing of the command value, two different approaches have been pursued. One method is to directly forward the unmodified $\Delta n_{Z,\mathrm{S}}$ command to the protection limiter. The other way is to feed the command signal through a shaping filter consisting of two sequential lead-lag shaping filters. The purpose of those shaping filters is to reduce or eliminate the attitude drop-back by modifying the $T_{\Theta 2}$ zero in the stick to attitude transfer function. The trade-off in diminishing the attitude drop-back is, however, a reduced bandwidth in the stick to flight-path angle transfer function. The shaping filters reduce the pitch rate overshoot $q_{\mathrm{peak}}/q_{\mathrm{SS}}$ in the stick to pitch rate transfer function. This functionality could also be achieved with one lead-lag filter alone. The second lead-lag filter is required to accelerate the initial response to a stick deflection to restore the CAP parameter as the pilot expects a proper correlation between the initial pitch rate acceleration and the resulting quasi-steady load factor response which is the interpretation of CAP.

An important aspect of the control design at hand is that the intervention of envelope protections and limitations is implemented by dynamic limiters to the upper and lower bound value of the normal command path $\Delta n_{Z,S}$. This means that if a protection or limitation requires a $\Delta n_{Z,\mathrm{S}}$ value smaller than that currently commanded by the pilot, the command value is reduced to the value provided by the limitation/protection. The same holds with regard to the lower limit. By that procedure, it is ensured that no transients occur when a protection becomes active. Furthermore, the protection stops to interfere with the pilot command as soon as the load factor increment commanded by the pilot no longer corresponds to a flight condition out of the protected envelope.

It is to be noted that when designing the different protection modes, the control variable available to the related feedback loops is no longer the elevator or a pitch control surface but a $\Delta n_{Z,S}$ command. The feedback treatment of the pitch axis protections and limitations will be described later in this section.

The output of the inner control loop is an elevator deflection command consisting of a superposition of the feed forward, the integral load factor feedback, and the proportional feedback of the load factor and the pitch rate. It is, on the one hand, directly sent to the elevator actuator and, on the other hand, slowly integrated to a stabilizer deflection. This procedure slowly moves the elevator back to zero deflection, producing the trim moment required for steady-state flight conditions with the use of the stabilizer. During transient flight manoeuvres and in protections, stabilizer integration is frozen as those conditions are not to be trimmed in terms of steady states.

4.2 Protection and limitation modes

So far, the descriptions have addressed the normal operation mode, i.e. the aircraft is in normal flight and none of the envelope limitations and protections are active. While mode activation criteria and transition/switching logics are to be detailed later, the system structure of the different protection modes and flight laws is presented in the following sections in the form of changes to the normal operating law and mode.

In the direct control law, the whole feed forward branch including the command shaping and limiting portions is bypassed and replaced by a direct mapping of pitch stick to elevator deflections using a look-up table. The manual elevator deflection command is augmented by rudimentary proportional load factor and pitch rate feedback to ensure sufficient short-period damping and natural frequency. The stabilizer auto-trim is deactivated in the direct control law, and manual stabilizer trim must be performed to eliminate steady-state pitch stick deflections.

The same direct link between pitch stick and elevator is active when the aircraft is on the ground.

During flare, the pitch integrator and the stabilizer are frozen and an additional high-pass filtered speed feedback is introduced. These steps are implemented to generate positive pitch stiffness comparable to an aircraft without an FCS and thus natural behaviour

during flare and landing. Without those measures, the neutral pitch stability provided by the FCS would eliminate the need for the pilot to continuously apply back pressure during flare and landing and thus require unnatural block-inputs at the pitch stick.

For the pitch angle limitation, the pilot command value for the load factor increment $\Delta n_{Z,S}$ is simply limited by a low-pass filtered feedback of the error between the actual pitch angle and the limit pitch angles. The maximum allowed load factor increment is computed from the upper pitch angle limit $\theta_{\max}$, and the lower bound for $\Delta n_{Z,S}$ is derived from the minimum pitch angle $\theta_{\min}$ to be maintained

$$\Delta n_{Z,\mathrm{C},\max/\min,\theta} = k_{n_{Z},\theta} \cdot (\theta_{\max/\min} - \theta) \tag{41}$$

Thus, at the boundaries of the intended pitch angle envelope, the $\Delta n_{Z,\mathrm{S}}$ is limited to zero, allowing only negative values for $\Delta n_{Z,\mathrm{S}}$ above the maximum pitch angle and positive values in the opposite case. As temporarily exceeding the intended pitch angle range does not pose immediate danger to the aircraft, slight excursions over the threshold values are allowed. However, it is ensured that the transient overshoots are only small and of short duration. Allowing these overshoots eliminates the need for early control system interference with the pilot commands when the aircraft is still in the permissible pitch attitude region.

As far as the angle of attack is concerned, the high AoA protection again limits the maximum $\Delta n_{Z,\mathrm{S}}$ to be commanded by the pilot as a function of the error between a commanded angle of attack α_{C} and the actual angle of attack α

$$\Delta n_{Z,\mathrm{C},\max,\alpha} = k_{n_{Z},\alpha} \cdot (\alpha_{\mathrm{C}} - \alpha) \tag{42}$$

For that purpose, the variable commanded by the stick deflection is switched from C* to α_{C}.

The commanded angle of attack α_{C} ranges from an α_{Prot} that is some degrees below the angle of attack for maximum lift for zero stick deflection up to an angle of attack $\alpha_{\max}$ slightly below the lift curve maximum for full stick aft deflection.

As not exceeding the maximum angle of attack is very important, no transient overshoots are allowed. Thus the angle of attack feedback is designed to feature a high bandwidth and to be very responsive. Furthermore, to ensure steady-state accuracy, the integral load factor error feedback is replaced by integral feedback of the angle of attack deviation. Furthermore, the same high-pass filtered speed feedback that has already been addressed in the pitch angle limitation is activated to produce a nose-down moment if the speed is rapidly bleeding and thus helps to avoid transient angle of attack overshoots. Furthermore, the stabilizer is frozen to ensure that it does not produce additional nose-up moments.

The overspeed protection is implemented in analogy to the high angle of attack protection. However, in this case, the load factor is lower bounded by the protection. The commanded velocity is linearly scaled between the maximum operating speed V_{MO} or maximum operating Mach number M_{MO} (whichever results in a smaller indicated air speed) for neutral pitch stick and the dive speed V_{D} or dive Mach number M_{D} for pitch stick full forward. The feedback signal used for the overspeed protection is the error between the commanded speed and the lead-lag filtered indicated airspeed. When the high-speed protection is active, the stabilizer auto-trim is frozen in the direction of nose-down moments to avoid trimming excessive speeds as steady-state flight conditions.

Figure 5 presents the principle of the limitations and protections restricting the range of allowed load factor increments to be commanded by the pilot.

The following considerations have been made to design the gains for the protection and limitation modes.

1. The speed feedback used during flare and high angle of attack protection features a gain of $\sqrt{2} \cdot Z_{\mathrm{U}}$, eliminating the phugoid influence from the stick to angle of attack transfer function response.
2. For the speed high-pass filter, a time constant of $T = 30$ s was chosen
3. The zero of the lead-lag filter for the overspeed protection is selected to be $T_{1,V} = 1/\omega_{\mathrm{n,Phugoid}}$ and the pole of the filter $T_{2,V}$ is selected to cancel the slowest zero of the commanded load factor to speed transfer function. This procedure has the effect that not the phugoid, but the short-period branches of the commanded load factor to speed transfer

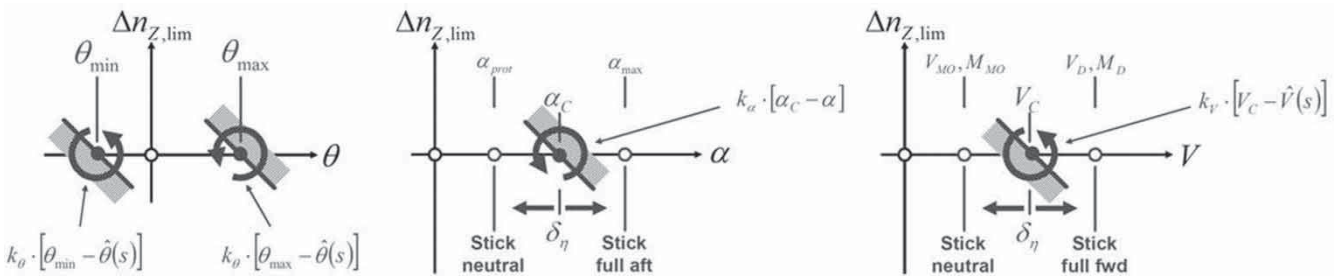

Fig. 5 Implementation of limitations/protections by dynamic command limiting

function root locus plot generate the asymptote running into the instable right half of the complex plane, allowing much higher speed feedback gains for tight speed tracking. For the final speed feedback gain of the overspeed protection, the gain value leading to the smallest imaginary part of the short-period poles is chosen.

4. The position of the pole of the pitch attitude limitation low-pass filter is chosen to cancel the zero of the load factor command to pitch attitude transfer function, which causes the short-period branches of the root locus to decrease the closed-loop damping.

A detailed description of the pitch control system can be taken from reference [**8**].

5 CONTROL SYSTEM IMPLEMENTATION

5.1 Non-linear compensations and couplings

In this section, aspects concerning couplings between pitch and lateral-directional control systems are addressed as well as implementation aspects dealing with the non-linear dynamics of the plant.

First of all, the stability axis load factor itself is not suitable for feedback as it has to be corrected for the trim contribution of the momentary flight condition. Thus, the load factor increment to trimmed flight to be used for feedback is computed as

$$\Delta n_{Z,\mathrm{S}} = n_{Z,\mathrm{S}} - \cos\gamma \cdot \cos\mu \tag{43}$$

where γ is the flight-path climb angle and μ the flight-path bank angle. The linear system models used for gain design are generated around straight and level flight, where gradients in load factor due to path and bank changes vanish in the system matrix. Thus, the effect of the non-linear term is not present during gain design but manifests in the flight-path angle, slowly drifting away from the steady-state value for non-horizontal flight conditions. The presence of the trim compensation removes this unintended effect. Furthermore, it is also possible to compensate for the change of the trim load factor by means of gravity rate compensation.

The next non-linear aspect is the turn compensation, which produces a load factor increment dependent on the flight-path bank angle that allows maintaining the actual path angle in the vertical plane without a requirement for the pilot to apply additional back pressure. The turn compensation term is computed as

$$\Delta n_{Z,\mathrm{Turn}} = \cos\gamma \cdot \frac{\sin^2\mu_{\mathrm{lim}}}{\cos\mu_{\mathrm{lim}}} \tag{44}$$

The subscript 'lim' indicates that the turn compensation is limited to a certain bank angle in the normal operating range. If the pilot intends to fly coordinated turns at higher bank, the additional load factor must actively be commanded.

The limit values for all relevant control variables are interpolated from tables that are dependent on configuration and flight conditions.

The coefficients of control system filters and feedback gains are scheduled dependent on free stream air density, dynamic pressure as well as estimated aircraft mass and C. G. location. For a later project stage, it is planned to try to increase the robust performance and stability of the system in order to eliminate the necessity of configuration-specific scheduling. At least as far as the lateral-directional control system is concerned, promising results have already been produced using multi-model eigenstructure assignment and iterative robustification methods based on singular value criteria and eigenvector orthogonalization.

All command and integration values are limited in the non-linear implementation of the FCS to avoid out-of-range commands and control surface saturation.

Supervisory mode control is performed by finite-state diagrams providing the following functionalities.

1. *Flight phase moding:* determination of the actual phase, either ground, flight, or flare based on ground contact, pitch angle, and radio altitude as well as on time intervals for which certain conditions have to apply.
2. *Flight control law moding:* determination of the main mode which can be fly-by-wire or direct law and for the fly-by-wire case also for the submode which can be normal operation or a reversionary mode with limited functionalities. In the simulation, the mode selection is not performed based on failure scenarios but actively triggered by the pilot.
3. *Speed feedback activation/deactivation:* activation of the high-pass filtered speed feedback as a function of the selected command law, the activation status of the angle of attack protection, and the current flight phase (speed feedback is active during flare).
4. *Stabilizer mode:* the activation/deactivation of the stabilizer auto-trim function is dependent on the activation status of envelope protections, the current command law, the flight phase, and the actual flight condition (transient manoeuvring or steady state).
5. *Control variable command:* current active control variable in the pitch and lateral control system dependent on control mode, flight phase, and protection activation.

Dependent on the system statuses listed above and the associated state transitions, the supervisory logics controls mode fadings, resets integrators, and blends command and control signals.

5.2 Implementation process

The FCS described in this article is implemented in SIMULINK following formal modelling style guidelines. The supervisory and mode logics are coded in the form of Stateflow charts. No numeric values are hard-coded in the models, but are transferred from the Matlab workspace using hierarchical workspace data structures.

Matlab design routines have been implemented to allow the automated generation of gain and coefficient tables from a grid of linearized system models, a handling qualities and control systems requirement definition file, and a design settings selection file. This process offers a high level of automation with only little user interaction required. This is pivotal for the simulation project as, on the one hand, model data and revisions rapidly change and, on the other hand, it is highly desirable to quickly evaluate the impact of changes in system requirements.

Automated linear assessment routines have been implemented to analyse linear system response in both time and frequency domains.

The scheme of the gain design process is depicted in Fig. 6. Whereas the structural layout of the control system is given by the functional requirements, the gain design is driven by two main requirement categories – handling qualities and stability.

One big advantage of the eigenstructure assignment-based process utilized here is that the handling qualities requirements can be deterministically assigned without requiring any iterations or tuning factors.

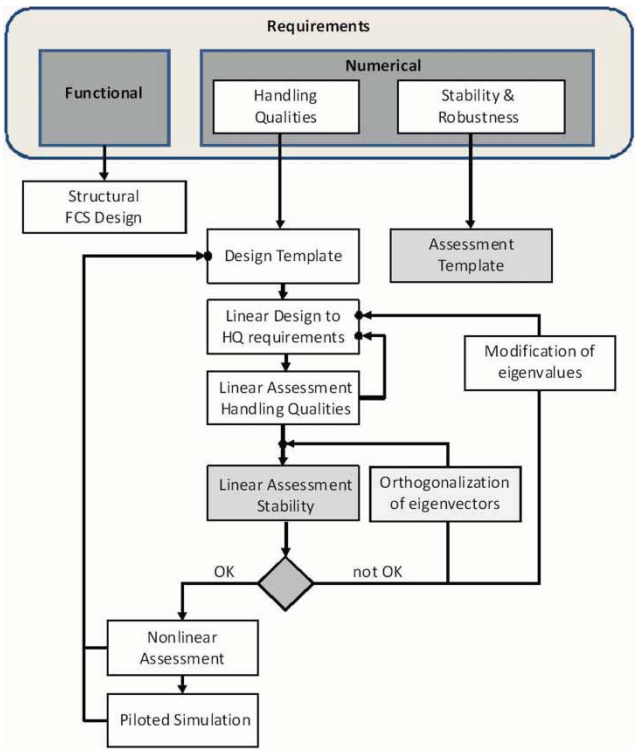

Fig. 6 Gain design iteration process

However, the mathematics of the algorithm does not directly incorporate the stability and robustness requirements into the process such that the resulting stability characteristics just become visible during linear assessment. At this point, the design iterations start.

First of all, it is iteratively attempted to increase system robustness by successive orthogonalization of the eigenvectors, reducing interactions between modes. However, if this does not produce sufficient stability margins, the specification of the exact location of the closed-loop poles must be sacrificed in favour of the stability requirements. For that purpose, the location of the design eigenvalues is adjusted by the algorithm detailed in section 3.3, where the distance of the selected eigenvalues from the desired ones is controlled via a user-selectable weighting matrix. By that means, handling qualities are traded for robustness. However, as pilot ratings remain rather constant in a significant range according to MIL-F-8785C and MIL-STD-1797A, this is an acceptable approach.

For time domain simulations, Real-Time Workshop and Stateflow Coder are used to automatically generate the C-Code of both the control system and the supervisory logics and to generate a library from that interim stage that can then be linked to the simulation executable. At the moment, the library is linked to a FORTRAN-based simulation model that is to be replaced by an all SIMULINK model currently under development.

6 ASSESSMENT

An analysis of the closed-loop dynamics based on the grid of linearized plant models is automatically performed to analyse the efficiency of the gain design process and to monitor the compliance of the resulting behaviour with the design requirements.

The effectiveness of the gain design procedure can be seen in Figs 7 and 8. The figures present the open-loop eigenstructure of the lateral rigid body states of a transport aircraft at Mach 0.7 in an altitude of 9000 m, yielding a weakly damped dutch roll and a spiral mode close to neutral stability.

For the closed-loop case, the eigenvalues are exactly at the desired locations, with the dutch roll featuring a damping of 0.7. The roll–yaw coupling has been completely removed, with the theoretical value of the bank angle remaining in the dutch roll eigenvector being around a numerical order of the numeric precision of the computer, i.e. 10^{-14}. The decoupling of roll and yaw dynamics is also visible in the spiral and roll mode eigenvectors where the angles of sideslip entries are effectively eliminated. Furthermore, the spiral pole is now at the desired fast location of -1.

Figure 9 illustrates the situation in the time domain as it presents the linear response of the

Eigenmode	Open-loop (x)	
	ζ [-]	ω_0 [rad/s]
1 – Roll Mode	1	1.3285
2 – Dutch Roll	0.12252	1.2053
3 – Spiral Mode	1	0.00098797

Eigenmode	Closed-loop (o)	
	ζ [-]	ω_0 [rad/s]
1 – Roll Mode	1	1.4286
2 – Dutch Roll	0.70711	2
3 – Spiral Mode	1	1

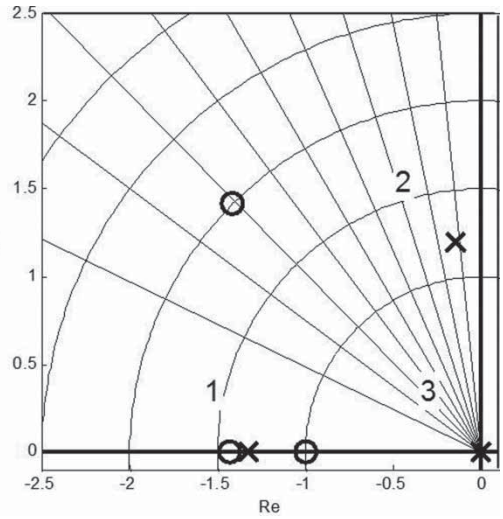

Fig. 7 Open- and closed-loop eigenvalues of lateral rigid body states ($Ma = 0.7$ and $h = 9000$ m)

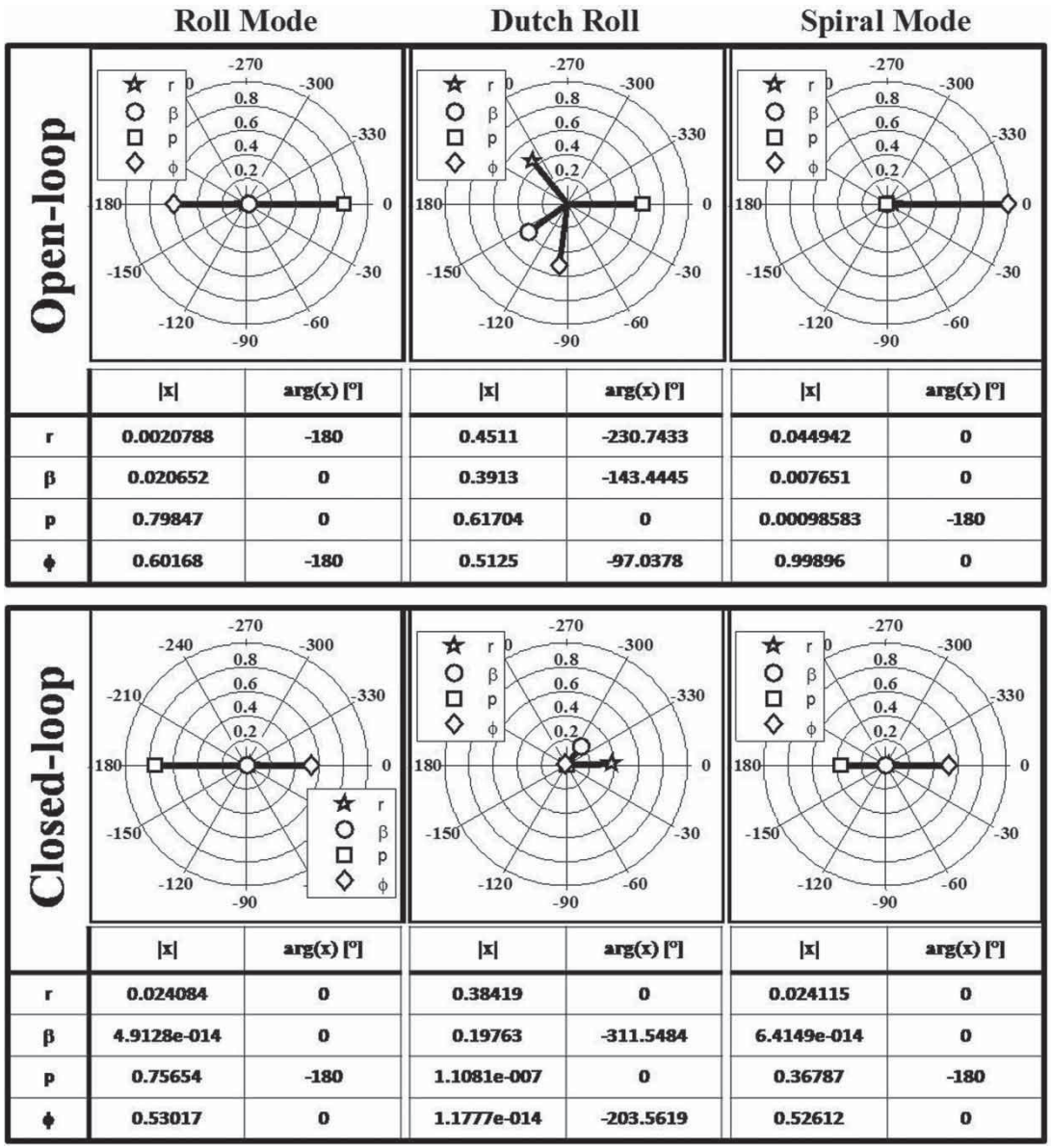

Open-loop	Roll Mode |x|	Roll Mode arg(x) [°]	Dutch Roll |x|	Dutch Roll arg(x) [°]	Spiral Mode |x|	Spiral Mode arg(x) [°]
r	0.0020788	-180	0.4511	-230.7433	0.044942	0
β	0.020652	0	0.3913	-143.4445	0.007651	0
p	0.79847	0	0.61704	0	0.00098583	-180
ϕ	0.60168	-180	0.5125	-97.0378	0.99896	0

Closed-loop	Roll Mode |x|	Roll Mode arg(x) [°]	Dutch Roll |x|	Dutch Roll arg(x) [°]	Spiral Mode |x|	Spiral Mode arg(x) [°]
r	0.024084	0	0.38419	0	0.024115	0
β	4.9128e-014	0	0.19763	-311.5484	6.4149e-014	0
p	0.75654	-180	1.1081e-007	0	0.36787	-180
ϕ	0.53017	0	1.1777e-014	-203.5619	0.52612	0

Fig. 8 Open- and closed-loop eigenstructure of lateral rigid body states ($Ma = 0.7$ and $h = 9000$ m)

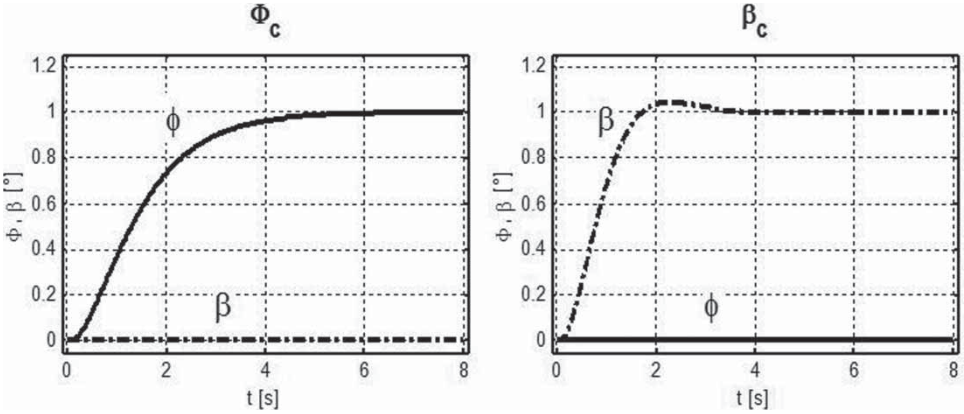

Fig. 9 Linear step response of lateral-directional states

lateral-directional states to steps in bank angle and angle of sideslip commands. The time histories again prove the quality of the decoupling between roll and yaw axis as for the bank angle command in the left column, no visible angle of sideslip is built up. The same holds for the sideslip command in the right column, where the bank angle resulting from the sideslip command is negligible. Furthermore, it is clearly visible that the linear dynamics of the closed-loop system reacts in compliance with the handling qualities criteria defined for the system. The roll rate rapidly builds up with the crisp roll time constant specified for the system, and the commanded bank angle is achieved aperiodically with the fast and stable spiral mode time constant specified for the inner loop. In the step response for the angle of sideslip, it is clearly visible that the latter one builds up with the required natural frequency and a light intentional overshoot related to the specified relative damping coefficient of $1/2 \cdot \sqrt{2}$.

The linear assessment, among others, includes state responses, analysed for decoupling, transient dynamics, and steady-state accuracy, and control and control rate responses, monitored for required control deflection budgets as well as control and rate saturation and to judge the overall control activity. Bode diagrams of the closed-loop responses from command variables to associated output are used to analyse steady-state accuracy, closed-loop bandwidth, high-frequency phase behaviour, and transient response amplitude peaks.

Some of the most important results of the linear assessment are that meeting the challenging time-constant requirements leads to significant control activity at low dynamic pressures associated with decreasing stability margins. This result supports the requirement to define the handling qualities as a function of the flight condition in contrast to requiring constant behaviour over the whole flight envelope. The high responsiveness and agility that can easily be achieved at high dynamic pressures cannot be produced with the required stability reserves at low dynamic pressures. Extending the dynamics that is possible at low speeds over the whole envelope would unnecessarily limit the manoeuvrability of the aircraft far below its physical capabilities, which are to be fully exploited for system-specific manoeuvres such as low-altitude flying. Another important result of the linear analysis is also the trade-off between pitch attitude drop-back and bandwidth of the stick to flight-path angle transfer function.

The pilot-in-the-loop simulations performed so far have successfully proved that the FCS design meets the specifications. Besides normal manoeuvres, formation flying and steep approaches have also been performed.

The fast integrator approach has not produced any PIO tendencies so far, even during formation flying in the presence of turbulence. On the other hand, the fast integrators lead to a quick and complete compensation of asymmetries, e.g. during simulated engine failures.

As far as pitch control is concerned, the presence of a head up display containing a flight-path marker leads to a pilot preference in high stick to flight-path angle response bandwidth in spite of significant associated attitude drop-back. Thus the drop-back reducing command shaping filter has been removed to account for this preference.

During rapid changes in thrust setting and the deployment of speedbrakes, the pitch control system slightly departs from the commanded flight-path angles, indicating that the fast integrator might not be sufficient to attenuate the effect of those rapid control movements. This might indicate the requirement for additional feed forward compensations to eliminate the transient excursions, although they are small and become apparent only in clinical still-air simulator conditions.

7 CONCLUSIONS AND PERSPECTIVES

Significant efforts have been made to implement a realistic FCS resembling the known or required

characteristics of the configuration to be analysed. Much attention was drawn to a high level of automation as far as gain and coefficient design is concerned to account for the rapid changes in model data, to fidelity as well as to the capability of rapidly analysing the effects of changes in requirements.

So far, especially the pilot simulations have proved that the system is suitable for the tasks to be performed. The next steps include analysis of specific manoeuvres such as low-altitude flying and the role of envelope protections and limitations on performing such manoeuvres. For example, one item will address the impact of pitch and bank angle limits during certain manoeuvres. Furthermore, it is intended to add the simulation of an auto-thrust system as well as of basic auto-pilot modes.

REFERENCES

1 **Brockhaus, R.** *Flugregelung*, 1994 (Springer, Berlin).

2 **Heller, M.** *Untersuchung zur Steuerung und Robusten Regelung der Seitenbewegung von Hyperschall-Flugzeugen*, 1999 (Herbert Utz Verlag, München).

3 **Faleiro, L.** *The application of eigenstructure assignment to the design of flight control systems*. Doctoral Thesis, Loughborough University, 1998.

4 **Farineau, J.** Lateral electric flight control laws of a civil aircraft based upon eigenstructure assignment technique. In Proceedings of the Guidance, Navigation and Control Conference, Boston, MA, August 1989, AIAA paper 1989-3594.

5 **Littleboy, D. M.** *Numerical techniques for eigenstructure assignment by output feedback in aircraft applications*. PhD Thesis, University of Reading, Department of Mathematics, 1994.

6 **Satoh, A.** and **Sugimoto, K.** Partial eigenstructure assignment approach for robust flight control. *J. Guid. Control Dyn.*, 2004, **27**(1), 145–150.

7 **Holzapfel, F., da Costa, O., Heller, M.,** and **Sachs, G.** Development of a lateral-directional flight control system for a new transport aircraft. In Proceedings of the Guidance, Navigation, and Control Conference, Keystone, CO, August 2006, AIAA paper 2006-6222.

8 **Holzapfel F., da Costa, O., Heller M.,** and **Sachs G.** Development of a longitudinal control system for a new transport aircraft. In Proceedings of the Guidance, Navigation and Control Conference, Keystone, CO, August 2006, AIAA paper 2006-6221.